

Kinetics and impacting factors of HO₂ uptake onto submicron atmospheric aerosols during a
2019 air quality study (AQUAS) in Yokohama, Japan

Jun Zhou^{a,b,c,*}, Kei Sato^d, Yu Bai^e, Yukiko Fukusaki^f, Yuka Kousa^f, Sathiyamurthi Ramasamy^d,
Akinori Takami^d, Ayako Yoshino^d, Tomoki Nakayama^g, Yasuhiro Sadanaga^h, Yoshihiro
Nakashimaⁱ, Jiaru Li^c, Kentaro Murano^c, Nanase Kohno^c, Yosuke Sakamoto^{c,d,e}, Yoshizumi
Kajii^{c,d,e,*}

^a Institute for Environmental and Climate Research, Jinan University, 511443 Guangzhou, China

^b Guangdong-Hongkong-Macau Joint Laboratory of Collaborative Innovation for Environmental Quality,
Guangzhou 511443, China

^c Graduate School of Global Environmental Studies, Kyoto University, Kyoto, 606-8501, Japan

^d Center for Regional Environmental Research, National Institute for Environmental Studies, Tsukuba, Ibaraki
305-8506, Japan

^e Graduate School of Human and Environmental Studies, Kyoto University, Kyoto 606-8501, Japan

^f Yokohama Environmental Science Research Institute, Yokohama Kanagawa 221-0024, Japan

^g Faculty of Environmental Science and Graduate School of Fisheries and Environmental Sciences, Nagasaki
University, Nagasaki 852-8521, Japan

^h Graduate School of Engineering, Osaka Prefecture University, Sakai, Osaka 599-8531, Japan

ⁱ Graduate School of Agriculture, Tokyo University of Agriculture and Technology, 3-5-8 Saiwai-cho, Fuchu,
Tokyo 183-8538, Japan

*Corresponding author.

Graduate School of Global Environmental Studies, Kyoto University, Kyoto 606-8501, Japan

E-mail address: kajii.yoshizumi.7e@kyoto-u.ac.jp and junzhou@jnu.edu.cn

Abstract

HO₂ uptake kinetics onto ambient aerosols play pivotal roles in tropospheric chemistry but are not fully understood. Field measurements of aerosol chemical and physical properties should be linked to molecular level kinetics; however, given that the HO₂ reactivity of ambient aerosols is low, traditional analytical techniques are unable to achieve this goal. We developed an online approach to precisely investigate the lower limit values of (i) the HO₂ reactivities of ambient gases and aerosols and (ii) HO₂ uptake coefficients onto ambient aerosols (γ) during 2019 air quality study (AQUAS) in Yokohama, Japan. We identified the effects of individual chemical components of ambient aerosols on γ . The results verified in laboratory studies on individual chemical components: transition metals play a key role in HO₂ uptake processes and chemical components indirectly influence such processes (i.e., through altering aerosol surface properties or providing active sites), with smaller particles tending to yield higher γ values than larger particles owing to the limitation of gas phase diffusion is smaller with micrometer particles and the distribution of depleting species such as transition metal ions is mostly distributed in accumulation mode of aerosol. The modeling of γ utilized transition metal chemistry derived by previous studies, further confirming our conclusion. However, owing to the high NO concentrations in Yokohama, peroxy radical loss onto submicron aerosols has a negligible impact on O₃ production rate and sensitivity regime.

1 Introduction

As an important atmospheric trace gas, the hydroperoxyl radical (HO₂) links many of the key oxidants in the troposphere, including the hydroxyl radical (OH), nitrate radical (NO₃⁻), ozone (O₃), and hydrogen peroxide (H₂O₂) (Logan et al., 1981; Chen et al., 2001; Jaeglé et al., 2000; Sommariva et al., 2004; Jacob, 2000). However, the observed HO₂ concentration in field measurements has not yet been fully explained by sophisticated models (known as the “HOx dilemma”) (Stone et al., 2012; Creasey et al., 1997; Kanaya et al., 2007b; Whalley et al., 2010; Millán et al., 2015), although it can be mostly solved in the conditions of clean marine air where NO concentration is low or aerosol loading is low

enough to make the heterogeneous reaction of HO₂ not important (Sommariva et al., 2004; Kanaya et al., 2007a). Owing to the short atmospheric lifetime of HO_x(=OH+HO₂+RO₂), the HO_x reactivity measurement can provide a robust test of its complex chemistry (Heard and Pilling, 2003). The HO₂ uptake kinetics onto ambient aerosols, including HO₂ reactivity (k_a) and uptake coefficient (γ), influence many atmospheric processes, including ozone formation rate, ozone formation sensitivity to NO_x, and H₂O₂ formation (Sakamoto et al., 2019; Thornton et al., 2008). With $\gamma > 0.1$, HO₂ concentration can also be influenced under conditions such as low [NO] or high aerosol loading (Lakey et al., 2015; Mao et al., 2013b; Martínez et al., 2003; Tie et al., 2001; Jacob, 2000; Matthews et al., 2014). These effects make the HO₂ uptake onto ambient aerosols indirectly influence human health and climate change.

From laboratory, field, and modeling studies, HO₂ uptake coefficients onto different types of aerosol can span several orders of magnitude (~ 0.002 – 1), which can be affected by many parameters, such as droplet/particle size and composition, the presence of dissolved reactive gases, and environmental conditions (i.e., relative humidity (RH), pH, and T) (Taketani et al., 2012; Taketani et al., 2008; Bedjanian et al., 2005; Thornton et al., 2008; George et al., 2013; Lakey et al., 2016a; Lakey et al., 2016b; Matthews et al., 2014; Cooper and Abbatt, 1996; Hanson et al., 1992; Thornton and Abbatt, 2005; González Palacios et al., 2016; Mozurkewich et al., 1987; Remorov et al., 2002; Jaeglé et al., 2000; Loukhovitskaya et al., 2009; Stone et al., 2012). In the absence of metals, the uptake of HO₂ by ambient aerosols is believed to occur *via* the acid–base dissociation of HO₂ ($\text{HO}_2(\text{g}) \leftrightarrow \text{HO}_2(\text{aq}); \text{HO}_2 \leftrightarrow \text{O}_2^- + \text{H}^+, pK_a = 4.7$), followed by electron transfer from O₂[−] to HO₂ (aq) ($\text{HO}_2 + \text{O}_2^- \xrightarrow{\text{H}_2\text{O}} \text{H}_2\text{O}_2 + \text{O}_2 + \text{OH}^-$), producing H₂O₂ (Jacob, 2000; Thornton et al., 2008; Zhou et al., 2019b). However, laboratory studies have shown that certain transition metals (i.e., Cu(II) and Fe(II)) can act as catalysts and accelerate HO₂ uptake rates onto many chemical compounds (Thornton et al., 2008; Taketani et al., 2008; Taketani et al., 2012, Cooper and Abbatt, 1996). Owing to the sufficiently high metal concentrations in tropospheric aerosols, as shown in previous field measurements (Hofmann et al., 1991; Wilkinson et al., 1997; Guieu et al., 1997; Manoj et al., 2000; Halstead et al., 2000; Siefert et al., 1998; Sedlak and Hoigné, 1993; Guo et al., 2014), recent studies have proposed that γ may be dominated by metals contained in the aerosol. This can lead to the HO₂ destruction (Mao et al., 2013a;

George et al., 2013), forming H_2O_2 , HO_2 -water complexes, or water and sulfate (Mozurkewich et al., 1987; Cooper and Abbatt, 1996; Gonzalez et al., 2010; Loukhovitskaya et al., 2009; Mao et al., 2010; Macintyre and Evans, 2011), which are important in the evolution of the chemical composition and physical properties of particles (George and Abbatt, 2010; George et al., 2008). The available data concerning HO_2 uptake kinetics onto ambient aerosols are insufficient for quantitative consideration owing to the much lower k_a value, as compared with the HO_2 reactivity of ambient gases (k_g). Therefore, they are below the detection limits of the current instruments.

To our knowledge, aside from us, only one study has measured γ , using an offline method that integrated ambient aerosols over size and time (Taketani et al., 2012). Considering that the offline method may distort γ , we developed an online approach to evaluate HO_2 uptake kinetics onto ambient aerosols. This method was successfully applied in Kyoto, Japan, in summer 2018, using a versatile aerosol concentration enrichment system (VACES) and a technique combining laser-flash photolysis with laser-induced fluorescence (LFP-LIF) (Zhou et al., 2019b). The obtained average γ value (~ 0.24) was comparable with the previous values used for modeling studies (~ 0.2) (Stadtler et al., 2018; Jacob, 2000). However, the large standard deviation (± 0.20 , 1σ) of γ along with the measurement time suggest that many other parameters might play a role, e.g., the measurement setup, aerosol characteristics, T , and RH.

In this study, we chose Yokohama (Japan), a coastal city with higher pollutant levels than Kyoto and different properties of the air masses from mainland Japan and the coast, as the measurement site. This is part of the Air QUALity Study (AQUAS) campaigns. The chemical and physical properties of ambient aerosols were quantified in real-time. To test their influence on k_a and γ , we conducted correlation matrix analysis coupled with the bootstrap method and classified the arriving air masses from different directions. Further, the main mechanism of γ was investigated by comparing the real-time quantified γ values with the modeled values. The impact of the peroxy radical's loss onto ambient aerosols on air quality is evaluated through their impact on ozone formation rates and their sensitivity to NO_x . The results obtained here will for better estimation of the heterogeneous reaction between HO_2 and ambient aerosols in sophisticated air quality models.

2 Materials and methods

2.1 Sampling sites

The measurement campaign was conducted at Yokohama Environmental Science Research Institute in Yokohama, Japan (location: 35°28'52.8"N, 139°39'30.3"E), from July 24 to August 03, 2019. The sampling ports of the instruments were placed approximately 25 m above the ground. Figure S1 shows the air mass directions during the campaign, which can be classified into two categories: (i) from the sea to the north, toward Yokohama City (~19% of the experimental period: from 12:00 July 25 to 12:00 July 27, 2019) and (ii) from the mainland toward Yokohama City (~81% of the experimental period). This classification was intended to distinguish the chemical properties of aerosols arriving from the mainland and the ocean, and to consequently quantify their impacts on k_a and γ .

2.2 Measurement strategies, instrumentation, and related data analysis

LFP-LIF In situ ambient air HO₂ reactivity was measured using LFP-LIF, which was adapted from a laser-induced pump and probe OH reactivity measurement technique. This approach has been successfully employed for gas and aerosol phase HO_x (=OH+HO₂) reactivity measurements (Sadanaga et al., 2004; Miyazaki et al., 2013; Sakamoto et al., 2018). Further details concerning the HO₂ reactivity measurements are described in the Supporting Information (SI).

VACES To compensate for the relatively low ambient aerosol concentrations thus the low k_a , and the low limit of detection (LOD) for the HO₂ reactivity measurement (~0.003 s⁻¹ with 240 decay integrations), a setup with VACES and an auto-switching aerosol filter was used before LFP-LIF. The VACES was built according to Sioutas et al. (1999), the ambient air sample was drawn into a tank (containing ultra-pure water heated up to ~32 °C) of VACES through a PM_{2.5} cyclone at a flow rate of over ~ 100 L min⁻¹, where the ambient air stream was saturated and subsequently cooled down in a condenser connected above the tank (with a temperature of -2 °C). During this process, the water droplets with diameters >2 μm formed on the collected ambient aerosols, which were then enriched by a virtual impactor (with a 50% cutoff point less than 1 μm) and dried by passing through a diffusion dryer connected right after the condenser in sequence. The concentration enrichment of the ambient

aerosols can be estimated using the total intake flow of VACES and the minor output flow of the virtual impactor that connected to the aerosol instrumentations (more details are given in SI: the enrichment of the ambient aerosols). Wang et al. (2013, 2014) claimed that when using the same technique as VACES for the online measurement of copper in ambient aerosols, equivalent copper concentrations were obtained compared to those measured by inductively coupled plasma mass spectrometer (ICP-MS) for both total and water-soluble components, which indicates the impact of VACES system to the solubility of Cu contained in ambient aerosol is negligible. Furthermore, previous studies found the liquid-liquid phase separation RH ranged from 60%-100% in atmospherically relevant particles consisting of organic species and inorganic salts (Yu et al., 2014), and the organic component appears to be the most useful parameter for estimating the liquid-liquid phase separation, which was always observed for oxygen-to-carbon elemental ratio (O:C) < 0.5 and was never observed for O:C ≥ 0.8 (Bertram et al., 2011). In this study, the ambient aerosol O:C ranged from 0.1 to 0.7, and the RH changing from ~80% (in ambient air) to >100% (in water tank), and then to ~75% (in reaction cell), suggest that the phase separation may have already happened before entering the VACES system, thus we assume the morphology of the ambient aerosols didn't change during the concentration enrichment process. Unfortunately, we did not measure the chemical composition after the VACES, thus we are not able to compare the chemical composition of the post VACES aerosols to ambient aerosol. However, previous test using the ambient aerosol fractions including coarse and fine PM indicated that the enrichment process of the VACES system does not differentially affect the chemical composition of ambient PM (Kim et al., 2001), thus we assume the chemical composition changing due to the enrichment process of the VACES can be neglected. The enrichment factor of the ambient aerosol surface area (E) was calculated from the difference between the surface areas measured before and after VACES by two scanning mobility particle sizers (SMPSs).

Aerosol physical properties and the enrichment factor of VACES The mass concentration and surface area of ambient aerosols (before VACES) were determined using a Scanning Mobility Particle Sizer (SMPS₁, model 3936L72, TSI, measure particle size distribution at 14.1–736.5 nm, 5-min intervals). The mass concentration of PM_{2.5} was measured using a palm-sized optical PM_{2.5} sensor (Nakayama et al., 2018). In order to test the enrichment factor of the VACES, a SMPS₂ (model 3936L75, TSI, measure particle size distribution at 14.6–661.2 nm, 5-min intervals) was used to measure the enriched mass

concentration and surface area of ambient aerosols (after VACES) for ~ 2 hours every day for ~ 6 days. The enrichment factor of VACES for the surface area was estimated as 12.5 ± 2.5 from the ratio between S_2 and S_1 , where S_2 and S_1 are the averaged surface areas measured by SMPS₂ and SMPS₁ of each day, respectively. According to the test from previous study of the VACES system, there is no distortion of the size distribution of the original ultrafine aerosols as the particle concentration enrichment occurs without any coagulation (Sioutas et al., 1999), here we listed the mean radius and geometric standard deviation (Geo. Std. Dev.) of the ambient aerosols before and after VACES during the enrichment factor measurement periods, as shown in Table 1. We could see that the mean radius before and after VACES are not statistically different within the standard deviation.

Table 1: The Mean radius and Geometric standard deviation of ambient aerosols before and after VACES

Experimental time•	Before VACES		After VACES	
	Mean radius (nm)	Geo. Std. Dev.	Mean radius (nm)	Geo. Std. Dev.
2019.7.25 09:03 – 11:03	129.47±11.32	0.92±0.04	133.19±3.37	0.92±0.02
2019.7.26 09:30 – 11:30	94.95±14.42	0.99±0.09	85.09±14.96	1.01±0.09
2019.7.27 10:00 – 12:00	85.09±14.96	1.01±0.09	80.40±21.01	1.01±0.07
2019.7.28 09:30 – 11:30	163.62±13.32	1.01±0.08	164.06±14.40	1.04±0.06
2019.7.29 09:10 – 11:10	128.06±6.90	0.91±0.02	125.07±7.68	0.92±0.02
2019.7.30 09:30 – 11:30	111.40±8.21	1.01±0.02	115.32±6.26	1.01±0.03

•represent the time period of the enrichment factor measurements;

±represent the standard deviation of the averaged values of mean radius and Geo. Std. Dev.

The enriched surface area of ambient aerosols with aerodynamic diameter $< 0.74 \mu\text{m}$ (PM_{0.74}) was calculated from the surface area of ambient aerosol measured by SMPS₁ and the enrichment factor. The enriched surface area of PM_{2.5} was then calculated by multiplying the enriched surface area of PM_{0.74} by the mass ratio between PM_{2.5} and PM_{0.75} (~1.1), where we assume the surface area are increased in proportional to the mass concentration. However, as the larger particles (here referred to particles ranged from 0.74 to 2.5 μm) tend to have lower surface area than the smaller particles, we consider the obtained enriched surface area of PM_{2.5} as the upper limit value. More details can be found in SI.

HO₂ uptake kinetics After passing through the VACES system, the ambient air was sampled using a three-port valve (Bolt, Flon Industry Co., LTD) and injected into the LFP–LIF system. The valve was switched automatically between two sampling lines, one with the aerosol filter on, and the other one

with the aerosol filter off, HO₂ reactivities in ambient air caused by two modes were measured: (a) the gas phase mode with aerosol filter on, the HO₂ reactivities are represented as k_g , and (b) the gas + enriched aerosol phase mode with aerosol filter off, the HO₂ reactivities are represented as $k_g + Ek_a$, where E represents the enrichment factor of k_a , Ek_a represents the total HO₂ reactivities caused by enriched ambient aerosols, the usage of Ek_a is based on the assumption that HO₂ uptake with aerosol particles follows the pseudo-first-order rate law. We modeled k_g in both modes using a theory identified previously (see SI: HO₂ reactivity of ambient gas phase) (Zhou et al., 2019b) and compared it with the measured values. The differences between measured and modeled k_g in mode (a) enabled us to establish their interrelationship and to check instrument stability. The differences between $(k_g + Ek_a)$ and the modeled k_g in mode (b) are considered as the enriched aerosol phase HO₂ reactivity (Ek_a). The total HO₂ reactivity decay profile follows single-exponential decay:

$$HO_2 = [HO_2]_0 \exp(-(k_g + Ek_a + k_{bg})t) \quad (1)$$

where k_{bg} denotes the zero air background obtained by injecting zero air with the same RH as the real-time ambient value into the reaction cell every 24 h for 30 min. The RH was controlled by passing some of the zero air through a water bubbler. The value of k_{bg} was subtracted separately on each day. The variability of k_{bg} (i.e., the reproducibility of the laser system) was calculated as the standard deviation of the response of repeated measurements on different days. It was found to be ~4%, which is slightly higher than the instrument precision (3%). A 30-min average calculation was applied to the data to reduce data fluctuation. The observed HO₂ uptake coefficients onto ambient aerosols (γ_{obs}) can be calculated from the dependence of Ek_a on γ_{obs} :

$$Ek_a = \frac{\gamma_{obs} \omega_{HO_2} ES}{4} \quad (2)$$

where ES and ω_{HO_2} represent the enriched surface area of ambient aerosol after VACES and the mean thermal velocity of HO₂ (~437.4 m s⁻¹), respectively. The uncertainty of the enriched surface area was estimated from the instrument systematic error of SMPS (~8%) and the uncertainty of the enrichment factor (± 2.5), which are shown in Fig.1b (see SI). The HO₂ reactivity of ambient aerosol (k_a) can be obtained from Ek_a by dividing by the enrichment factor E .

High resolution–time of flight–aerosol mass spectrometry (HR–ToF–AMS) A field-deployable HR–ToF–AMS (Aerodyne Research Inc.) (DeCarlo et al., 2006) was used for the characterization of the non-refractory aerosol mass with a time resolution of ~3 min. The HR–ToF–AMS measured the total organic aerosol (OA), sulfate (SO_4^{2-}), nitrate (NO_3^-), ammonium (NH_4^+), chloride (Cl^-), and the two most dominant oxygen-containing ions in the OA spectra, i.e., mass-to-charge ratios of $m/z = 44$ (Org44, mostly CO_2^+) and $m/z = 43$ (Org43, mainly $\text{C}_2\text{H}_3\text{O}^+$ for the oxygenated OA and C_3H_7^+ for the hydrocarbon-like OA) (Ng et al., 2011). The fractions of Org44 and Org43 in OA are represented as f_{44} and f_{43} , respectively. Ambient air was sampled through a critical orifice into an aerodynamic lens, which efficiently transmitted particles between 80 nm and up to at least 1 μm . Particles were flash-vaporized by impaction on a resistively heated surface (~600 °C) and ionized by electron ionization (70 eV). The m/z values of the resulting fragments were determined using a ToF mass spectrometer. Data were analyzed using the ToF–AMS software SQUIRREL and PIKA. Data were not corrected for lens transmission efficiency. Standard relative ionization efficiencies (RIE) were used for organics (RIE = 1.4), nitrate (RIE = 1.1), chloride (RIE = 1.3), sulfate (RIE = 1.12), and ammonium (RIE = 4). Concentration data were obtained from background-subtracted stick-mass data (low-mass-resolution-base mass concentration data, which are calibrated using ammonium sulfate particles) and determined assuming a collection efficiency (CE) of 0.5.

Filter-based photometer Real-time measurement of the equivalent black carbon (eBC) was performed using a 5-wavelength dual-spot absorption photometer (MA300, AethLabs, San Francisco, CA, USA), which performed an online correction for possible artefacts resulting from filter loading and multiple scattering (Drinovec et al., 2015). In this study, eBC data obtained from light attenuation at a wavelength of 880 nm were used to avoid possible contributions from brown carbon; the time resolution was ~1 min.

Trace elements Fourteen trace elements (Al, V, Cr, Mn, Co, Ni, Cu, Zn, As, Se, Sr, Cd, Ba, and Pb) were measured using an offline method at two-day intervals from 21 July to 5 August 2019. The suspended particulate matter (SPM) was collected onto 623.7 cm^2 size quartz fiber filters (Pallflex Tissuquartz 2500QAT-UP), which had an available collecting area of 405.84 cm^2 , using a high-volume

sampler (1000 L min^{-1}). Approximately 2 cm^2 of each filter was cut into pieces and placed into a polytetrafluoroethylene (PTFE) pressure digestion tank with 1 mL 49% hydrofluoric acid (HF) and 5 mL 69% nitric acid (HNO_3). A Thermo Fisher X2 Series ICP–MS was then used to determine metal concentrations. By assuming that the metal fractions were the same in SPM and PM_{10} (aerosol particles with aerodynamic diameters less than $1 \mu\text{m}$), the concentrations in PM_{10} were estimated according to the tested metal concentrations in SPM and the ratio between SPM and PM_{10} measured in situ.

Water-soluble inorganic species NR- PM_{10} water-soluble inorganic species (including Na^+ , SO_4^{2-} , NH_4^+ , NO_3^- , Cl^- , Ca^{2+} , K^+ , Mg^{2+}) used for the *ISORROPIA-II* model were also measured using offline method, as described above. For extraction, we cut 1/4 of a 47 mm filter punched from the original collected filter and placed it in 10 mL of ultrapure water (18.2 MW cm^{-1}) in a centrifuge tube. This was followed by 15 min of ultrasonication in a 30°C water bath. The solution was then vortexed (Vortex Genie 2, Scientific Industries, USA) for 1 min to ensure homogeneity and filtered through syringe filter with pore size of $0.45\text{-}\mu\text{m}$ (Advantec Dismic-25, PTFE). An Ion Chromatograph (IC, ICS1600, DIONEX, USA) was employed to determine the concentrations of these inorganic ions in the extracted solution.

Gas phase monitors NO_2 was measured by cavity attenuated phase shift (CAPS, Aerodyne Research, USA, at 1-s intervals), $\text{NO}_y\text{--NO}$ by chemiluminescence (Model 42i-TL, Thermo, at 10-s intervals), CO by Thermo CO analyzer of nondispersive infrared spectroscopy (Model 48i-TLE, Thermo Scientific, USA, at 10-s time intervals), and O_3 by UV absorption (Model 1150, Dylec, AMI Co., Ltd, at 10-s time intervals). HCHO was determined by high performance liquid chromatography (HPLC; 1260 Infinity, Agilent Technologies Inc, USA) from 14:00 July 29, to 12:00 August 3, 2019. An average value of $\sim 2 \text{ ppb}$ was used for the data analysis.

ISORROPIA-II model NR- PM_{10} water-soluble inorganic species (including Na^+ , SO_4^{2-} , NH_4^+ , NO_3^- , Cl^- , Ca^{2+} , K^+ , Mg^{2+}) and meteorological parameters including temperature and RH were used to calculate the aerosol pH and liquid water content based on the *ISORROPIA-II* model (Fountoukis and Nenes, 2007). We ran *ISORROPIA-II* in “reverse” mode and the particles were assumed to be deliquescent, i.e.,

in metastable mode (Hennigan et al., 2015). The thermodynamic equilibrium of the $\text{NH}_4^+ - \text{SO}_4^{2-} - \text{NO}_3^-$ system case was used for modeling.

3 Results and discussion

3.1 The HO_2 uptake kinetics onto ambient aerosols

The measured total HO_2 reactivities were compared against the modeled gas phase HO_2 reactivity under the experimental conditions both with and without the aerosol phase. Without the aerosol phase, the modeled k_g values are calculated according to the description in Sect. 2.2, which are not statistically different with the measured k_g values (Fig. 1a second panel, T-test, $p = 0.49$, with inspection level = 0.05), indicating that HO_2 loss in the reaction cell was dominated by its reaction with NO_2 in the LFP-LIF system. With the aerosol phase, the measured ($Ek_a + k_g$) and modeled values ($\approx k_g$) were significantly different (see Fig. 2b, first panel, T-test, $p = 0.04$, with inspection level = 0.05). The differences were considered to be the HO_2 reactivities of enriched ambient aerosols (Ek_a). Ek_a ranged between 0.015 s^{-1} (25th percentile) and 0.097 s^{-1} (75th percentile), with the median value of 0.059 s^{-1} , the corresponding k_a , calculated by dividing Ek_a by E , ranged between 0.001 s^{-1} (25th percentile) and 0.008 s^{-1} (75th percentile), with the median value of 0.005 s^{-1} and average value of $0.005 \pm 0.005 \text{ s}^{-1}$. The error for Ek_a was estimated as $\sim 0.05 \text{ s}^{-1}$, calculated as the propagated error from $k_g + Ek_a$ (i.e., the systematic error of the instrument, $\sim 0.05 \text{ s}^{-1}$) and the modeled k_g in mode (b) ($\sim 0.001 \text{ s}^{-1}$). The error for k_a was then estimated as $\sim 0.004 \text{ s}^{-1}$ by dividing the error of Ek_a by the enrichment factor E . The corresponding γ , calculated from Eq. 2, ranged from 0.05 (25th percentile) to 0.33 (75th percentile), with the median value of 0.19 (with an average value of 0.23 ± 0.21). The mean diameter of ambient particles ranged from 0.1 to $0.46 \mu\text{m}$ (with the median value of $0.25 \mu\text{m}$), the gas-phase diffusion effects on γ were estimated to be $\sim 6.6 \%$ (further details are given in the SI). The absolute increase of γ due to the gas-phase diffusion is 0.03 on average, which is negligible compared to γ uncertainty (~ 0.21 on average). Therefore, we ignored the gas-phase diffusion effects to γ .

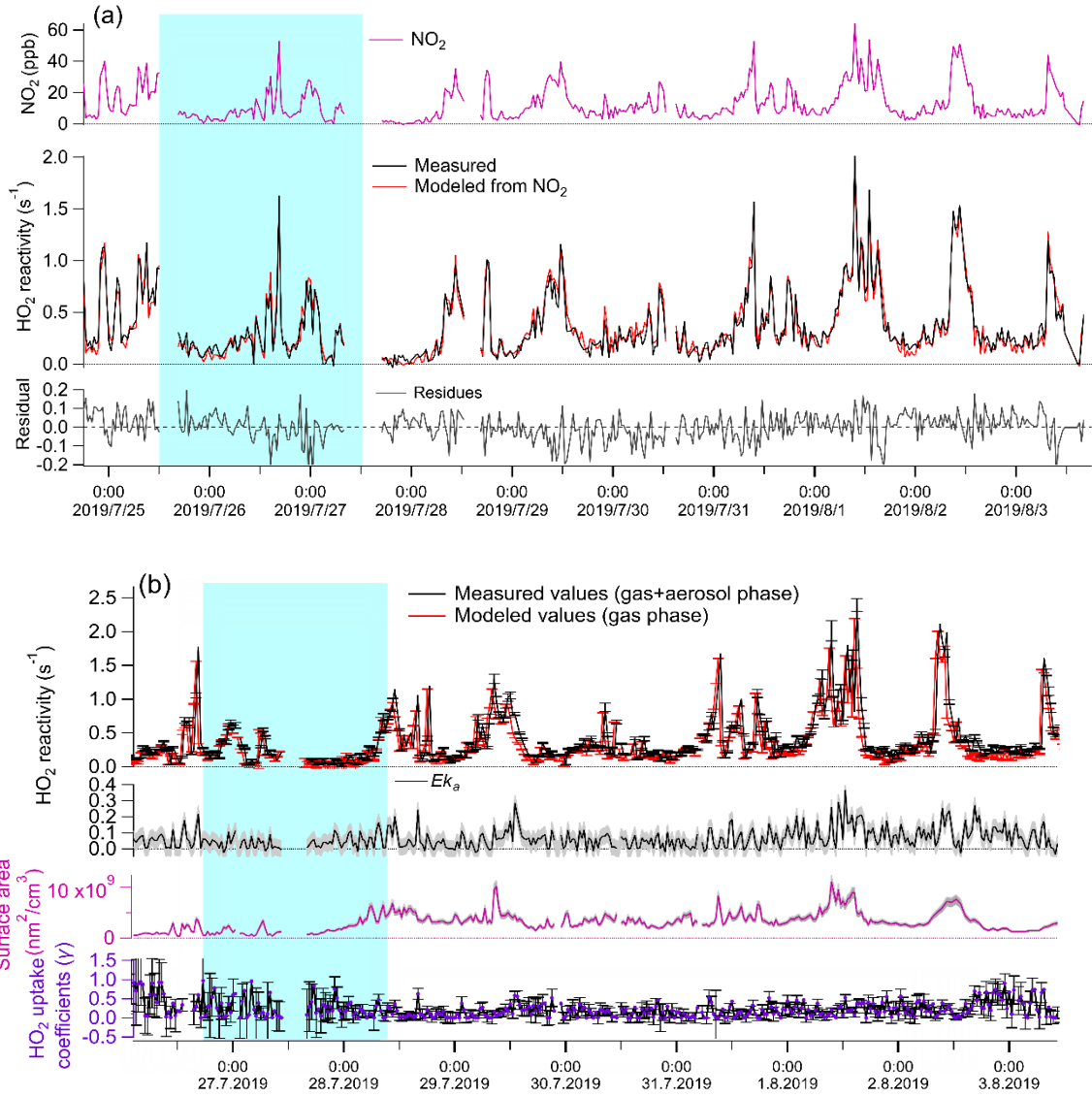


Figure 1: Temporal variation of parameters under different experimental conditions. (a) Without aerosol phase: 1st panel: measured NO₂ concentrations (ppb); 2nd panel: measured (red line) and modeled (black line) k_g ; 3rd panel: fitting residues of modeled k_g values, ranging from -0.04 (25 percentile) to 0.05 (75 percentile), therefore we consider the systematic error of the LFP-LIF instrument to be $\sim 0.05 \text{ s}^{-1}$. (b) Gas + aerosol phase: 1st panel: measured total HO₂ reactivity ($k_g + Ek_a$) and modeled k_g ; 2nd panel: Ek_a , calculated from the difference between the measured and modeled values from the 1st panel, the gray shadow area represents the uncertainty of Ek_a (ΔEk_a), propagated from the error of ($k_g + Ek_a$) and modeled k_g ; 3rd panel: the upper limit surface area of the enriched ambient aerosols (ES), the gray shadow area represents the uncertainty of ES (ΔES), propagated from the systematic errors of the SMPS instrument ($\sim 8\%$), and the uncertainty of the enrichment factor; 4th panel: γ calculated from Ek_a and ES according to Eq. 2. The errors for γ were propagated from ΔEk_a and ΔES , $\Delta \gamma = \gamma \times \sqrt{\frac{\Delta Ek_a^2}{Ek_a^2} + \frac{\Delta ES^2}{ES^2}}$. The blue shaded area represents the air masses from group i (from coast), the remainder is from group ii (from mainland).

Statistical significance analysis showed that the average γ value of group i (0.35 ± 0.28) is significantly higher than that of group ii (0.21 ± 0.16) (calculated $p = 4.9\text{E-}5$; Mann-Whitney), indicating that the air masses from the ocean yield higher γ values than the air masses from mainland Japan. The difference in γ values between group i and group ii may due to the different chemical

components contained in the ambient aerosols arrived from the ocean or mainland, which we will discuss in the following sections. The average value of k_a at Yokohama ($0.005 \pm 0.005 \text{ s}^{-1}$) was much higher than that at Kyoto city ($0.0017 \pm 0.0015 \text{ s}^{-1}$) (with calculated $p < 0.05$; Mann-Whitney), this may be due to the different aerosol properties in Kyoto and Yokohama city. We list some of them as follows:

- 1) mass composition, the aerosols at the coast city (Yokohama) tend to contain more sea salts thus increased k_a ,
- 2) particle size distribution, smaller particles tend to yield higher γ values than larger particles owing to the depleting species (e.g., transition metal ions) are mostly distributed in accumulation mode of aerosol,
- 3) the water content and the metal concentrations, which will highly influence the HO_2 uptake capacity of the ambient aerosols. However, the average value of HO_2 uptake coefficient onto ambient aerosols (γ) at Yokohama is ~ 0.23 , which is comparable with previous measured ($\sim 0.24\text{--}0.25$) (Zhou et al., 2019b; Taketani et al., 2012) and modeled (~ 0.20) values (Stadtler et al., 2018; Jacob, 2000). The large standard deviation (± 0.21 , 1σ) of the values along with the measurement time may be due to the instantaneously changed chemical and physical properties of ambient aerosols, indicating that a large bias may exist if a constant γ value is used for modeling.

3.2 Bulk chemical composition of ambient aerosols

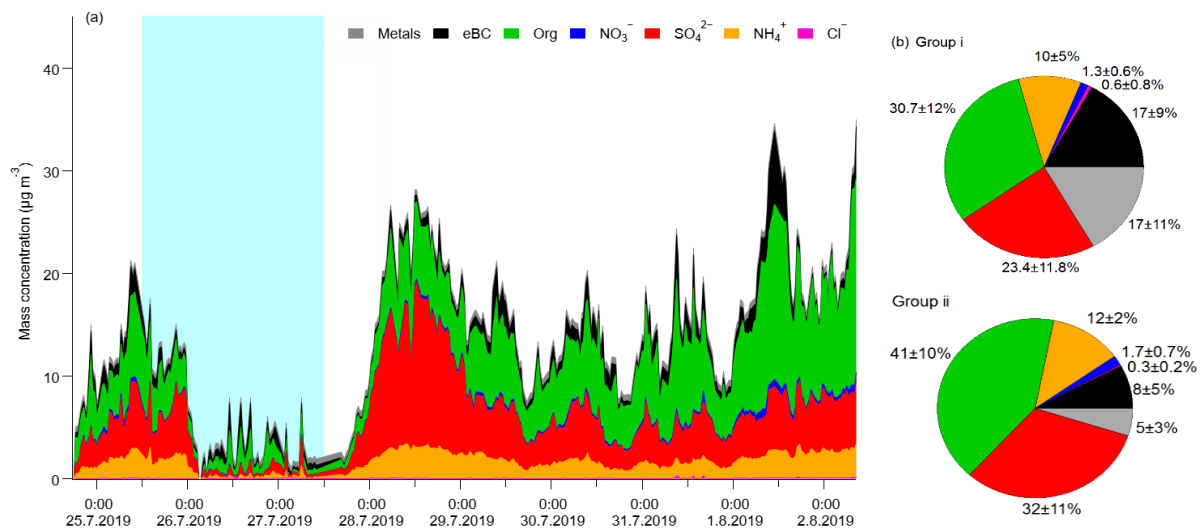


Figure 2: (a) Concentrations of non-refractory chemical components plus eBC in Yokohama, Japan (July 24 to August 02, 2019). The blue shaded area represents group i from coast and the remaining areas represent group ii from mainland. (b) Average contribution fractions of different chemical components of groups i and ii.

Figure 2a shows the time series of the mass concentrations of OA, SO_4^{2-} , NO_3^- , NH_4^+ , Cl^- , and eBC in PM_{10} in Yokohama from July 24 to August 02, 2019, which is ~ 1.5 days less than for the LFP–LIF data.

During this period, PM_{10} ranged from ~ 1 to $35 \mu g m^{-3}$ (average $\approx 13 \mu g m^{-3}$) and was dominated by OA, SO_4^{2-} , and NH_4^+ , with contributions of $39 \pm 11\%$, $30 \pm 12\%$, and $12 \pm 4\%$, respectively; these were followed by eBC and metals, with contributions of $10 \pm 7\%$ and $8 \pm 8\%$, respectively. Cl^- contributed $< 1\%$ in both groups, which is similar to that reported for an urban area in winter in Bern (Switzerland) (Zhou et al., 2019a). However, NO_3^- contributed much less ($\sim 2 \pm 0.7\%$) compared with that reported for Bern ($\sim 19 \pm 4\%$), which may be due to the reverse reaction of NH_4NO_3 converting to HNO_3 . Since Yokohama is a coastal city, and HNO_3 is easily vaporized in summer, gaseous HNO_3 may sink with sea salt particles by forming $NaNO_3$ through heterogeneous reactions (Finlayson-Pitts and Pitts, 2000).

Figure 2b shows the average contribution fractions of different components of group i and group ii. The main differences in the components between these two groups are the fractions of OA, BC, SO_4^{2-} , and metals. The OA fraction was ~ 1.8 and ~ 8.4 times higher than that for the metals in groups i and ii, respectively. As OA can cover the surface of the particles and thereby decrease γ (Lakey et al., 2016a; Takami et al., 2013), the difference between the OA and metal fractions in these two groups may partially explain the much higher γ values of group i (vs. group ii). Previous studies have shown quite low HO_2 uptake coefficient on BC (~ 0.01) (Saathoff et al., 2001; Macintyre and Evans, 2011), which is different with the result obtained here. This may be due to the much higher fraction of BC in group i (vs. group ii) provide active sites for HO_2 self-reaction or its reaction with the H atom from the abstraction reaction from hydrogen containing functional groups and form H_2O_2 (Bedjanian et al., 2005), or BC can be coated with additional materials (e.g., sulfate and organic carbon) thus influence HO_2 uptake (Schwarz et al., 2008). We also observed slightly higher Cl^- and BC fraction in group i (from ocean) than that in group ii (from mainland), which may be due to the effects of sea salt and the ship emissions in the air mass from the ocean, respectively. From the average diurnal patterns (Figs. S5 and S6), the trends in k_a follow the trends in chemical composition, whereas γ shows a contrasting trend with both variables in both groups. For group ii, SO_4^{2-} and OA exhibited higher values whereas γ exhibited lower values during the daytime than those during nighttime, indicating that secondary aerosol formation resulting from photochemical reactions may decrease γ . To identify the influence of each

individual chemical component of ambient aerosol on k_a and γ , we further performed correlation matrix analysis.

3.3 Influence of individual chemical components of ambient aerosol on k_a and γ

For multiple-component ambient aerosol, k_a and γ are influenced by different chemical components, these chemical components may also have mutual effects to each other, for example, the transition metal Cu and Fe contained in ambient aerosols can be chelated by organics (Lakey et al., 2016b). Therefore, we produced a Pearson correlation matrix of all the testing factors at Yokohama city, including different chemical components, k_a and γ . Here we note that the different chemical components were measured using HR-ToF-AMS for ambient aerosols with aerodynamic diameters $< 1 \mu\text{m}$, while k_a and γ were measured using VACES-LFP-LIF system for ambient aerosols with aerodynamic diameters $< 2.5 \mu\text{m}$, but due to most “fine-mode” aerosols have the mean diameter ranged from $0.09 \mu\text{m}$ to $0.47 \mu\text{m}$ (with the median value of $0.25 \mu\text{m}$, measured by SMPS), we assume the chemical components of ambient aerosols with the aerodynamic diameter ranged between $1 \mu\text{m}$ and $2.5 \mu\text{m}$ have negligible impact on Pearson correlation matrix result. However, present results do not include the effects of coarse particles (with aerodynamic diameters $> 2.5 \mu\text{m}$) to the HO_2 uptake kinetics, and we may partially miss measuring sea spray (with diameters ranged from ~ 0.05 to $10 \mu\text{m}$) effects. When Cl^- measured by AMS increased, coarse particles may exist and our results may not represent the real ambient conditions. Consequently, we consider our results as the lower limit of the HO_2 uptake kinetics onto real ambient aerosols.

To exclude the effects of the different fractions of chemical components in groups i and ii, the bootstrap method, which is based on the creation of replicate the inputs by perturbing the original data through resampling, was employed. The resampling was performed by randomly reorganizing the rows of the original time series such that some rows of the original data were present several times while other rows were removed. The final results were obtained by running the data for 1000 bootstrap replicates. The average values of these 1000 bootstrap replicates are listed in Fig. 3.

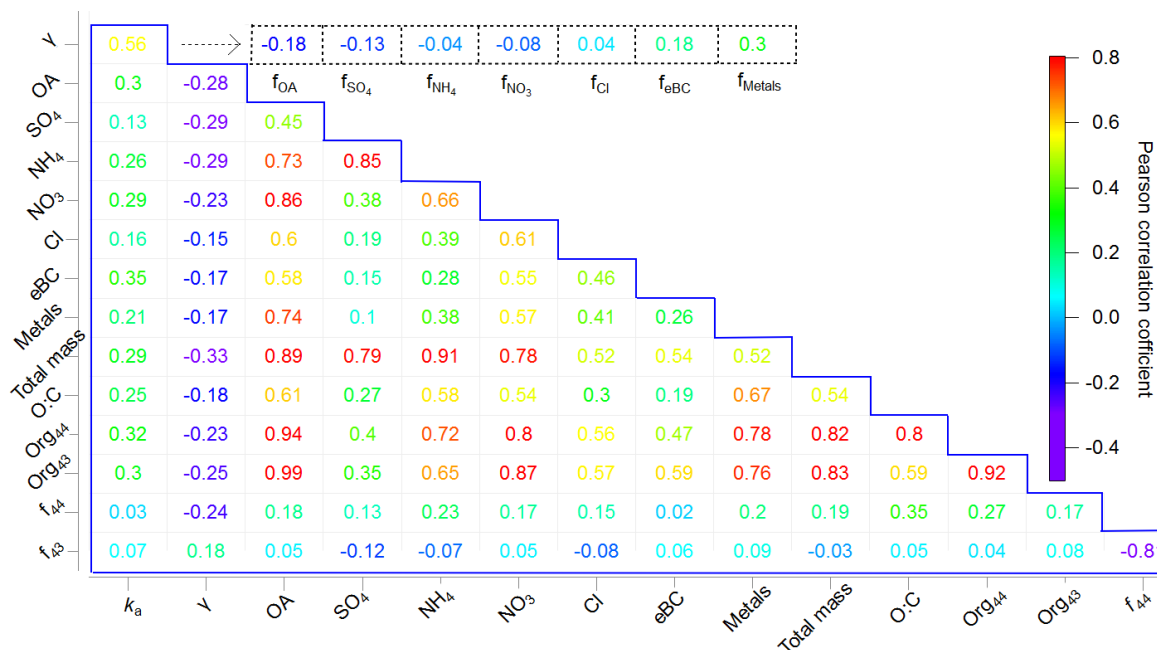


Figure 3: Correlation matrix showing Pearson's r values for the chemical compositions, k_a , and γ during the corresponding measurement periods (in the blue box), as well as the Pearson's r values for the chemical composition fraction i (represented as f_i , $i = \text{OA}, \text{SO}_4^{2-}, \text{NH}_4^+, \text{NO}_3^-, \text{Cl}^-, \text{eBC}$, and metals) and γ (in the dashed line box).

Most of the chemical components had strong or moderate Pearson correlation coefficients with each other (Fig. 3), although k_a and γ showed only a moderate correlation with each other (0.56). As γ can be correlated with the qualitative, rather than quantitative, properties of the aerosols, we further investigated the Pearson's r values between the chemical composition fractions and γ . The results show that k_a was positively correlated with total mass and the individual chemical components, whereas γ showed only a weak positive correlation with f_{metals} (0.30) and f_{eBC} (0.18). According to previous studies, metals may act as a catalyst thus accelerating the depletion of HO_2 (Mao et al., 2013a), and BC can provide active sites or can be coated by other chemical components thus facilitating the HO_2 uptake (Bedjanian et al., 2005; Schwarz et al. (2008), as described in Sect.3.2. The very weak correlation of γ with f_{Cl^-} (0.04) may be related to Cl^- chemistry, for example, $\text{HO}_2(\text{g})$ can react with $\text{NaCl}(\text{g})$, produce NaOH and $\text{Cl}_2(\text{g})$, thus cause a decrease in the HO_2 concentration and indirectly effects γ (Remorov et al., 2002). Interestingly, when considering the Org₄₄ and Org₄₃ fractions in total OA separately, γ is positively correlated with f_{43} (0.18) but negatively correlated with f_{44} (-0.24). This is consistent with previous conclusion that more oxidized organic aerosols tend to be highly viscous and thus decrease HO_2 uptake coefficients (Lakey et al., 2016b). In summary, γ was dominated by the free forms of

transition metals that can act as catalysts of HO₂ uptake onto ambient aerosols, and was indirectly affected by chemical components that might alter the properties of ambient aerosols, e.g., oxygenated OA can cover the aerosol surface and alter the viscosity of ambient aerosols, thereby decrease γ (Lakey et al., 2016a; Lakey et al., 2016b; Takami et al., 2013), whereas BC may provide active sites or be coated by other chemical components, thereby increase γ . This is further confirmed by the classification of the air masses, i.e., the air mass from the ocean (group i), which contained less OA and more metals than that from mainland Japan (group ii), had a higher HO₂ uptake capacity. We further compared the measured γ values with the modeled γ values using previously proposed mechanisms, as shown below.

3.4 Possible mechanism of HO₂ uptake onto ambient aerosols

Two mechanisms of HO₂ uptake onto aqueous ambient aerosols have been proposed, for which equations have been derived from a previous study (Thornton et al., 2008): (i) HO₂-only chemistry and (ii) chemistry with transition metals playing a role. In this study, the liquid content of the total ambient aerosol mass ranged from 70% to 88%, as obtained from the *ISORROPIA-II model*. As the solubility of Fe is rather small in ambient aerosol, the reaction rates of Fe/Mn for liquid phase HO₂ in aerosol is ~ 100 times slower than it is for Cu, thus the influence of Fe and Mn on HO₂ uptake can be neglected compared to Cu or scaled as equivalent [Cu²⁺] (Fang et al., 2017; Hsu et al., 2010; Baker and Jickells, 2006; Oakes et al., 2012; Song et al., 2020), therefore, we use the soluble Cu as surrogate for transition metals in ambient aerosols to assess their influence to γ . The Cu solute mass fraction in the liquid content of the ambient aerosols was estimated as $(3.5\text{--}30) \times 10^{-4}$ mol L⁻¹ according to our offline filter test (Sect. 2.2), and to get the effective concentrations of Cu ions which can participate in the reaction of the destruction of peroxy radicals, the activity coefficient for total Cu was assumed to be 0.1 (upper limit) based on a study of (NH₄)₂SO₄ particles at 68% RH (Ross and Noone, 1991; Robinson and Stokes, 1970). Using copper ions as a surrogate metal for transition metal ions (TMIs), the potential HO₂ loss onto aqueous ambient aerosols via mechanisms involving TMIs was estimated as (Hanson et al., 1994):

$$\frac{1}{\gamma_{\text{TMI}}} = \frac{1}{\alpha^{\text{HO}_2}} + \frac{\omega}{H_{\text{eff}}RT\sqrt{k^{\text{I}}D_{\text{aq}}Q}}, \quad (3)$$

where α^{HO_2} is the mass accommodation coefficient of HO_2 , ω is the mean HO_2 molecular speed (cm s^{-1}), H_{eff} is the effective Henry's Law coefficient, R is the gas constant ($\text{J K}^{-1} \text{mol}^{-1}$), and T the temperature (K). k^{I} is the pseudo-first-order rate constant equal to $k_{\text{TMI}}^{\text{II}}[\text{TMI}]$, where $k_{\text{TMI}}^{\text{II}}$ is the second order rate constant for aqueous phase reaction with HO_2/O_2^- and TMI. Q' accounts for aqueous-phase diffusion limitations and is expressed as

$$Q' = [\coth(q) - \frac{1}{q}]; q = r_p \sqrt{\frac{k^{\text{I}}}{D_{\text{aq}}}} \quad (4)$$

Table S1 shows more details of the parameters used for modeling. Previous laboratory studies suggest the mass accommodation coefficient for various single-component aerosols doped with Cu(II) is commonly > 0.2 (Taketani et al., 2008, 2009; Mozurkewich et al., 1987; Thornton and Abbatt, 2005; George et al., 2013; Lakey et al., 2016a, 2016b), and organics substantially reduce HO_2 uptake onto aerosols containing TMI (Lakey et al., 2016b). Here we calculated γ^{TMI} with $\alpha^{\text{HO}_2}=0.2$ using Eq. 3, which are plotted in Fig. 4a along with the measured γ values; the much lower variation of the modeled values may due to the low time resolution (~ 2 days) of $[\text{Cu}]$. The measured γ values (~ 0.23 on average) are significantly higher than the modeled γ^{TMI} with $\alpha^{\text{HO}_2}=0.2$ (~ 0.16 on average), with calculated $p < 0.05$ (t-test), which may due to the TMI contained in the ambient aerosol. However, when using the upper limit of the mass accommodation value for modelling (with $\alpha^{\text{HO}_2}=1$), the measured γ values are significantly lower than the modelled γ^{TMI} (averaged value: ~ 0.50), these results indicating that the chemical components may be internally mixed, as proposed by Takami et al. (2013), which influences the aerosol surface tension and the activity of the free form of the copper ion (i.e., OA and BC) to constrain γ^{TMI} . We suggest that the additional collective effects of different chemical components to α^{HO_2} and the bulk reactions should be involved in the γ^{TMI} modelling to get accurate estimation. No linear correlation was found between γ^{TMI} and γ . Further classification of measured $\gamma \geq 0.4$ and $\gamma < 0.4$ shows that γ^{TMI} has a weak correlation with measured γ values when $\gamma \geq 0.4$ (Fig. S7), which may due to the higher fraction of metals in the total mass at measured $\gamma \geq 0.4$ ($\sim 12\%$) than at < 0.4 ($\sim 7\%$); therefore, the impact of the other chemical components is much lower. The γ values obtained here are comparable with those in previous ambient aerosol studies (Taketani et al., 2008; Zhou et al., 2019b) (Fig.

5b). When compare with single-compound aerosols obtained from laboratory studies, γ values were generally higher than the HO₂ uptake coefficients onto organic species (Lakey et al., 2015), soot particles (Bedjanian et al., 2005), and the dry state of inorganic aerosols (i.e., (NH₄)₂SO₄, NaCl, and H₂SO₄), but comparable or lower than aqueous and copper-doped aqueous phases of inorganic species (Fig. 4b) (George et al., 2013; Lakey et al., 2016b; Taketani et al., 2008; Thornton and Abbatt, 2005). This may indicate the collective effects of the individual chemical components of ambient aerosols to γ , and the significant influence of RH to aerosol states of single-component particles thus their HO₂ uptake coefficients.

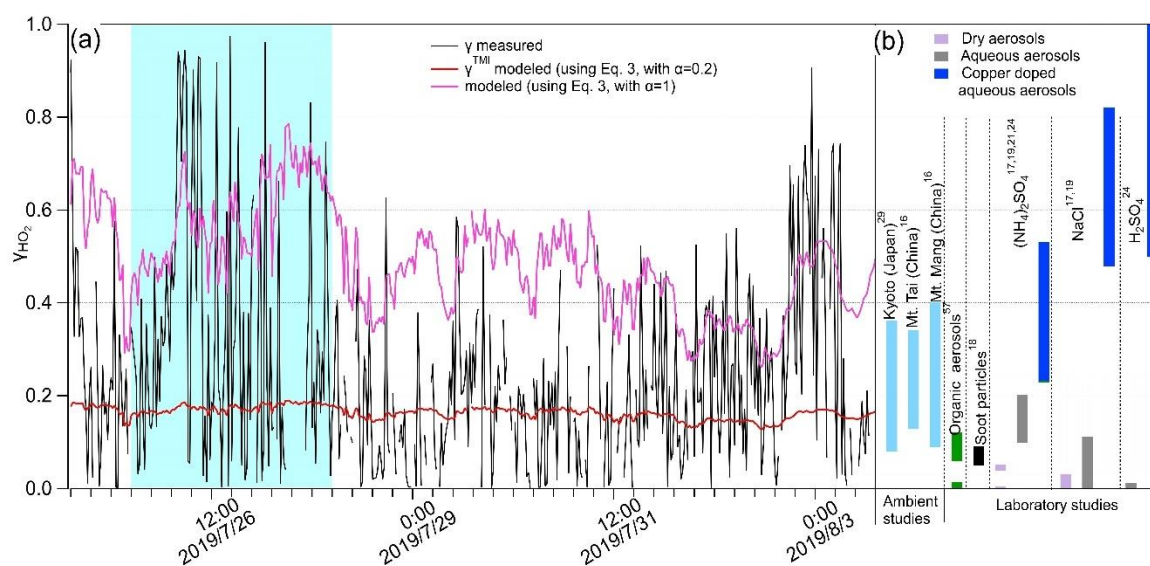


Figure 4: (a) Measured and modeled γ values along with measurement time. The blue shaded area represents group i; the remaining areas represent group ii. (b) HO₂ uptake coefficients onto different types of aerosol obtained from ambient and laboratory studies, the numbers indicate the related references from which the data were obtained: 1. Zhou et al., 2019b; 2. Taketani et al., 2012; 3. Lakey et al, 2015; 4. Bedjanian et al., 2005; 5. Taketani et al., 2008; 6. George et al., 2013; 7. Lakey et al., 2016b; 8. Thornton and Abbatt, 2005.

Other studies have shown that γ is strongly negatively temperature dependent (Remorov et al., 2002; Mao et al., 2010; Cooper and Abbatt, 1996; Hanson et al., 1992; Thornton and Abbatt, 2005; Gershenzon et al., 1995). Here, RH and T were stabilized by the VACES–LFP–LIF system (in the reaction cell), as compared with those in ambient air (Fig. S8), statistical analysis indicates the RH and T in the reaction cell were on average decreased 3.3% (T-test, $p < 0.05$, with inspection level = 0.05) and 2.3 °C (T-test, $p < 0.05$, with inspection level = 0.05), compared to that in ambient air, respectively, which is much smaller than the standard deviation of T and RH (which are ~3.7 °C and 16.4%, respectively) along with the measurement time. We noticed that k_a and γ showed no dependence on RH and T in the

reaction cell (see Fig. S9), indicating that the instantaneous change of RH and T may not be the dominating factors in terms of the variation of k_a and γ with measurement time, and the stabilization of RH and T by VACES–LFP–LIF system have negligible effects to k_a and γ . This suggests that the individual chemical components and physical properties of ambient aerosols may dominate γ variation during field campaign; both the metal-catalyzed reactions and the chemical components and their states should be considered to yield more accurate γ values. Results obtained here are in accordance with previous results on correlations between particulate H_2O_2 (which can be formed by the uptake of HO_2) and coarse particulate transition metals (Wang et al., 2010). Using an offline methodology to investigate the influence of RH and T by maintaining constant experimental conditions or chemical compositions will be the subject of future work.

3.5 Influence of the physical properties of ambient aerosols on k_a and γ

HO_2 heterogeneous loss rates are driven by the different particle sizes of different aerosol types (i.e., urban ambient aerosols and marine aerosols)(Morita et al., 2004; Guo et al., 2019; Jacob, 2000). In this study, k_a and γ showed no linear dependence on the mean ambient particle diameters (see Fig. S10). Identifying the fractional contributions of aerosols in different particle size ranges to k_a and γ is highly desirable in terms of understanding their influence. However, it seems that high γ values (> 0.8) occur when the surface area is $< 2 \times 10^{-6} \text{ cm}^2 \text{ cm}^{-3}$ and the mean particle diameter is $< 110 \text{ nm}$. This is in accordance with a previous study showing that aerosols yield the highest fractional contribution to the total heterogeneous loss rate of HO_2 radicals of size $< 0.1 \mu\text{m}$ (Morita et al., 2004) and that the mass accommodation process plays the determining role for small and medium sized aerosols in controlling HO_2 uptake. Guo et al. (2019) states the HO_2 radicals experience less loss upon its diffusion into larger droplets than its diffusion into small droplets due to dilution effects make the larger aerosols having lower depleting species concentrations (Cu^{2+}). However, this was based on the assumption that the total mass of Cu^{2+} is constant during the hygroscopic growth of particles which is not always true in the ambient conditions. Further studies about Cu^{2+} content in particles with different sizes are needed to fully understand the result here.

3.6 Significance of k_a to O_3 formation potential

In urban atmosphere, XO_2 ($=HO_2+RO_2$) fate is important to the photochemical production of ozone ($P(O_3)$). Here, the loss rates of XO_2 due to three factors were compared: (i) uptake onto the ambient aerosols (L_{P-XO_2} in Eq. 5), since no experiment or reference available for RO_2 uptake onto ambient particles, we assume the RO_2 reactivities caused by its interaction with ambient aerosols were the same as k_a , (ii) XO_2 self-reactions (L_{R-XO_2} in Eq. 6), and (iii) reaction with NO (L_{N-XO_2} in Eq. 7), which can produce NO_2 , a precursor of O_3 ; therefore Eq. 7 can also be regarded as $P(O_3)$.

$$L_{P-XO_2} = k_a[XO_2] \quad (5)$$

$$L_{R-XO_2} = 2 * (k_{HO_2-HO_2}[HO_2]^2 + k_{HO_2-RO_2}[HO_2][RO_2]) \quad (6)$$

$$L_{NO-XO_2} = k_{NO-XO_2}[NO][XO_2] = P(O_3) \quad (7)$$

where $k_{HO_2-HO_2}$ and $k_{HO_2-RO_2}$ are the second-order rate constants of HO_2 self-reaction and its reaction with RO_2 , respectively. k_{NO-HO_2} is the second-order rate constant of the reaction of HO_2 with NO. The HO_2 concentration was estimated from O_3 concentration using the method described by Kanaya et al., (2007a). The RO_2 concentration is then estimated by assuming a steady state of HO_2 in the HO_x cycle; the reaction rates of HO_2 radicals are approximated as 0:

$$\begin{aligned} \frac{d[HO_2]}{dt} &= P_{HO_2} - L_{HO_2} = k_{CO-OH}[OH][CO] + k_{H_2CO-OH}[OH][H_2CO] + k_{NO-RO_2}[RO_2][NO] - \\ &2k_{HO_2-HO_2}[HO_2][HO_2] - k_{HO_2-RO_2}[HO_2][RO_2] - k_{NO-HO_2}[HO_2][NO] - k_a[HO_2] = 0 \end{aligned} \quad (8)$$

where k_{CO-OH} and k_{H_2CO-OH} are the second-order rate constants of the reactions of CO and H_2CO with OH, respectively. The different XO_2 loss rates described in Eqs. 5–7, along with the measurement times, are shown in Fig. 5a. Generally, L_{P-XO_2} is much greater than L_{R-XO_2} , indicating that the XO_2 taken up by ambient aerosols will compete with the XO_2 self-reaction, thus influencing XO_2 concentration. However, such an influence may have a negligible impact on $P(O_3)$ because L_{P-XO_2} is tens of thousands of times lower than L_{NO-XO_2} owing to the relatively high NOx concentration at Yokohama. We further tested the impact of L_{P-XO_2} on ozone formation sensitivity regime, according to the method proposed by Sakamoto et al. (2019), in which L_N/Q is used as a new indicator:

$$\frac{L_N}{Q} = \frac{1}{1 + \left(\frac{(2k_R[XO_2] + k_a')k_{OH-VOCs}[VOCs]}{(1-\alpha')k_{NO-HO_2}[NO]k_{OH-NO_2}[NO_2]} \right)} \quad (9)$$

where $k_{\text{OH-VOCs}}$ and $k_{\text{OH-NO}_2}$ are the second-order rate constants of the reactions of OH with VOCs and NO_2 , respectively. $k_{\text{NO-HO}_2}$ is the second-order rate constant of the reaction of NO with HO_2 . α' is the proportion of RO_2 in XO_2 . L_N is the OH radical loss rate through its reaction with NO_2 . ($= k_{\text{OH-NO}_2}[\text{OH}][\text{NO}_2]$), and Q is the total loss of the HOx radicals in the HOx cycle reaction ($= L_N + L_{\text{P-XO}_2} + L_{\text{R-XO}_2}$). The regime transition point can be expressed as

$$\frac{L_N}{Q_{\text{transition}}} = (1 - \chi)\frac{1}{2} + \chi\frac{1}{3} \quad (10)$$

where $\chi = L_{\text{P-XO}_2} / (L_{\text{P-XO}_2} + L_{\text{R-XO}_2})$. The results indicate that both L_N/Q and $L_N/Q_{\text{without_aerosol}}$ (calculated with and without including k_a' in Eq. 9, respectively) were higher than $L_N/Q_{\text{transition}}$, indicating that ozone formation was VOC-sensitive throughout the campaign and that the aerosol uptake of XO_2 (k_a') showed no impact on the O_3 formation regime (see Fig. 5, here we only consider the daytime, when photochemical reactions occur). The plots of L_N/Q and $L_N/Q_{\text{without_aerosol}}$ as a function of NO concentration show the values were closer to $L_N/Q_{\text{transition}}$ (~ 0.4) at lower NO concentrations (Fig. S11); therefore, aerosol uptake may play a more important role in the O_3 formation regime at NO levels lower than those observed in this study. The temporal variations in key factors used in this section are shown in Fig. S12.

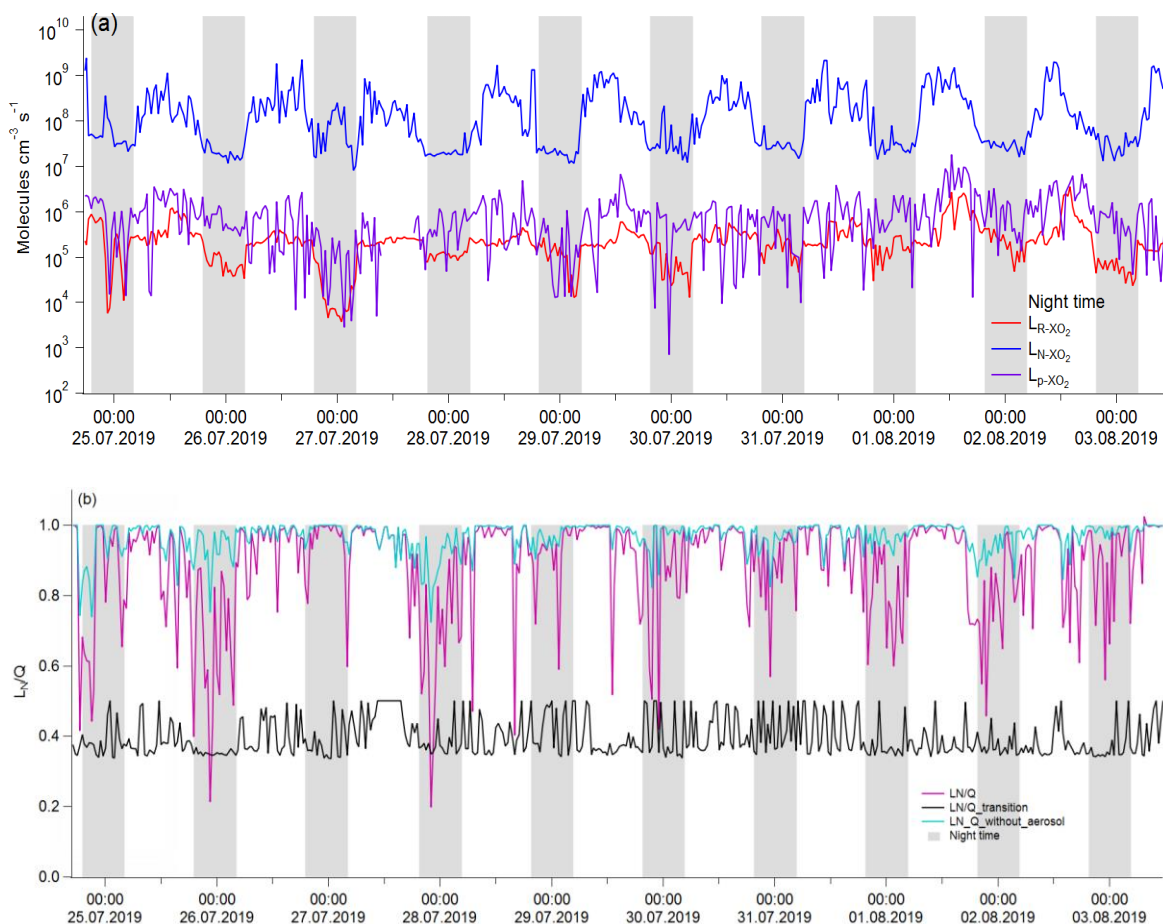


Figure 5: Temporal variations in (a) HO₂ radical loss rates and (b) L_N/Q (red line) and the regime transition threshold (L_N/Q_{transition}, black line) used to assess the ozone sensitivity regime. The gray shaded areas represent nighttime (from National Astronomical Observatory of Japan) and are not discussed herein.

4 Conclusions

This study used a reliable online methodology to investigate HO₂ uptake kinetics onto in situ ambient aerosols (i.e., HO₂ reactivity of ambient aerosols k_a and HO₂ uptake coefficients γ) and discussed the impacting factors on such processes, i.e., chemical compositions and physical properties of ambient aerosols and experimental conditions. k_a ranged between 0.001 s⁻¹ (25th percentile) and 0.005 s⁻¹ (75th percentile), with an average value of 0.005 ± 0.005 s⁻¹. The corresponding γ , ranged from 0.05 (25th percentile) to 0.33 (75th percentile), with the median value of 0.19 and the average value of 0.23 ± 0.21 , is comparable with previous measured (~ 0.24 – 0.25) (Zhou et al., 2019b; Taketani et al., 2012) and modeled (~ 0.20) values (Stadtler et al., 2018; Jacob, 2000). However, the k_a and γ values obtained here

are considered as the lower limit values for real ambient aerosols, as the coarse particles were not measured in this study. We noticed that k_a and γ showed no dependence on RH and T in the reaction cell in this study, indicating that the instantaneous change of RH and T may not be dominating factors in terms of the variation of k_a and γ with measurement time, and the large standard deviation of the γ values along with the measurement time (± 0.21 , 1σ) may be due to the instantaneously changed chemical and physical properties of ambient aerosols, a large bias may exist if a constant γ value is used for modeling.

We found that the individual chemical components of ambient aerosols may have collective effects of to γ , through the analyses of 1) separating the air masses into two groups, group i from the ocean and group ii from mainland Japan; 2) the average diurnal patterns; 3) the correlation matrix analysis of each individual chemical component of ambient aerosol with k_a and γ , and 4) the modeling studies using previously proposed mechanisms. All these efforts clearly indicating that the transition metals contained in ambient aerosols may act as a catalyst, thus accelerating the depletion of HO_2 , however, they can be chelated by OA. OA can also cover the aerosol surface and alter the viscosity of ambient aerosols, thereby decreasing γ , and that more oxidized organic aerosols tend to be highly viscous thus decrease HO_2 uptake coefficients. Results obtained here are in accordance to previous laboratory and modeling studies (Mao et al., 2013a; Lakey et al., 2016b; Lakey et al., 2016a; Takami et al., 2013; Thornton et al., 2008; Hanson et al., 1994). The chemical components of ambient aerosols may be internally mixed, as proposed by Takami et al. (2013), which influences the aerosol surface tension and the activity of the free form of the copper ion (i.e., OA and BC) to constrain γ . In contrast to previous studies saying that BC may shrink HO_2 losses onto ambient aerosols (Saathoff et al., 2001; Macintyre and Evans, 2011; Bedjanian et al., 2005), we found BC positively correlated with HO_2 uptake coefficients (0.18), this may be owing to BC can provide active sites or be coated by other chemical components thus facilitating the physical uptake of HO_2 . Here, we observed higher γ values (> 0.8) when the mean particle diameter is < 110 nm, identifying the fractional contributions of aerosols in different particle size ranges to k_a and γ is highly desirable in terms of understanding their influence.

In summary, the chemical components and physical properties of ambient aerosols may dominate

γ variation during field campaign; to yield more accurate γ value, total suspended particles in ambient air should be measured, and the metal-catalyzed reactions, chemical components, and aerosol states should be considered. Also, improvements to the time-resolution of metal measurements are needed for more precise analysis. For more detailed investigation of HO₂ uptake mechanisms, an offline methodology that can maintain constant chemical compositions and experimental conditions (such as RH and T) will be useful. The HO₂ loss onto ambient aerosols was identified to have a negligible impact on the O₃ production rate and formation regime owing to the high NO_x concentrations at Yokohama. This process may play a more important role in O₃ formation under low NO_x concentration and high aerosol loading conditions. The results help us to understand the impacts of HO₂ uptake kinetics on chemical transformations in troposphere.

Appendix:

Air mass directions (Figure S1), measurement strategy (Figure S2), a technique combined laser-flash photolysis with laser-induced fluorescence (LFP-LIF), the enrichment of the ambient aerosols, HO₂ reactivity of ambient air, correction of gas-phase diffusion for HO₂ uptake coefficient, HO₂ reactivity of ambient gas phase (k_g), examples of HO₂ decay profiles (Figure S3), HO₂ reactivity calibration with different NO₂ concentrations (Figure S4), diurnal trends in individual chemical components of ambient aerosols (Figure S5), diurnal trends in k_a and γ (Figure S6), correlations between measured and modeled γ (Figure S7), time series of the averaged RH and T in ambient air and the reaction cell (Figure S8), dependence of k_a and γ on RH in reaction cell (Figure S9), dependence of k_a and γ on mean particle diameter (Figure S10), dependence of day time LN/Q and LN/Q_without_aerosol on [NO] (Figure S11), profiles of key factors determining XO₂ loss rates and P(O₃) sensitivity (Figure S12), summary of equations and values used for γ modeling (Table S1), summary of equations and values used for XO₂ (=HO₂+RO₂) loss and O₃ formation sensitivity regime (Table S1).

Author contribution

J.J., K.M., Y.S., and Y.K. designed the experiments and J.J. and Y.B. carried them out. J.J. did the data analysis and prepared the manuscript with contributions from all co-authors.

Competing interests

The authors declare that they have no conflict of interest.

Data availability

Data supporting this publication are available upon request for the corresponding author (junzhou@jnu.edu.cn).

Acknowledgments

This work was supported by the Japan Society for the Promotion of Science (JSPS) KAKENHI Grant Numbers JP16H06305, JP19H04255. Many thanks to Yokohama Environmental Science Research Institute utility during the campaign.

References

- Baker, A. R., and Jickells, T. D.: Mineral particle size as a control on aerosol iron solubility, *Geophys. Res. Lett.*, 33, 10.1029/2006GL026557, 2006.
- Bertram, A. K., Martin, S. T., Hanna, S. J., Smith, M. L., Bodsworth, A., Chen, Q., Kuwata, M., Liu, A., You, Y., and Zorn, S. R.: Predicting the relative humidities of liquid-liquid phase separation, efflorescence, and deliquescence of mixed particles of ammonium sulfate, organic material, and water using the organic-to-sulfate mass ratio of the particle and the oxygen-to-carbon elemental ratio of the organic component, *Atmos. Chem. Phys.*, 11, 10995–11006, 10.5194/acp-11-10995-2011, 2011.
- Bedjanian, Y., Lelièvre, S., and Le Bras, G.: Experimental study of the interaction of HO₂ radicals with soot surface, *Phys. Chem. Chem. Phys.*, 7, 334–341, 10.1039/B414217A, 2005.
- Chen, G., Davis, D., Crawford, J., Heikes, B., O'Sullivan, D., Lee, M., Eisele, F., Mauldin, L., Tanner, D., Collins, J., Barrick, J., Anderson, B., Blake, D., Bradshaw, J., Sandholm, S., Carroll, M., Albercook, G., and Clarke, A.: An assessment of HO_x chemistry in the tropical pacific boundary layer: comparison of model simulations with observations recorded during PEM Tropics A, *J. Atmos. Chem.*, 38, 317–344, 10.1023/A:1006402626288, 2001.
- Cooper, P. L., and Abbatt, J. P. D.: Heterogeneous Interactions of OH and HO₂ Radicals with surfaces characteristic of atmospheric particulate matter, *J. Phys. Chem.*, 100, 2249–2254, 10.1021/jp952142z, 1996.
- DeCarlo, P. F., Kimmel, J. R., Trimborn, A., Northway, M. J., Jayne, J. T., Aiken, A. C., Gonin, M., Fuhrer, K., Horvath, T., Docherty, K. S., Worsnop, D. R., and Jimenez, J. L.: Field-Deployable, High-Resolution, Time-of-Flight Aerosol Mass Spectrometer, *Anal. Chem.* 78, 8281–8289, 10.1021/ac061249n, 2006.

Drinovec, L., Močnik, G., Zotter, P., Prévôt, A. S. H., Ruckstuhl, C., Coz, E., Rupakheti, M., Sciare, J., Müller, T., Wiedensohler, A., and Hansen, A. D. A.: The "dual-spot" Aethalometer: an improved measurement of aerosol black carbon with real-time loading compensation, *Atmos. Meas. Tech.*, 8, 1965-1979, 10.5194/amt-8-1965-2015, 2015.

Fang, T., Guo, H., Zeng, L., Verma, V., Nenes, A., and Weber, R. J.: Highly acidic ambient particles, soluble metals, and oxidative potential: a link between sulfate and aerosol toxicity, *Environ. Sci. Technol.*, 51, 2611-2620, 10.1021/acs.est.6b06151, 2017.

Finlayson-Pitts, B. J., and Pitts, J. N.: CHAPTER 7 - Chemistry of inorganic nitrogen compounds, in: chemistry of the upper and lower atmosphere, edited by: Finlayson-Pitts, B. J., and Pitts, J. N., Academic Press, San Diego, 264-293, 2000.

Fountoukis, C., and Nenes, A.: ISORROPIA II: a computationally efficient thermodynamic equilibrium model for K^+ - Ca^{2+} - Mg^{2+} - NH_4^+ - Na^+ - SO_4^{2-} - NO_3^- - Cl^- - H_2O aerosols, *Atmos. Chem. Phys.*, 7, 4639-4659, 10.5194/acp-7-4639-2007, 2007.

George, I. J., and Abbatt, J. P.: Heterogeneous oxidation of atmospheric aerosol particles by gas-phase radicals, *Nature chem.*, 2, 713-722, 10.1038/nchem.806, 2010.

George, I. J., Matthews, P. S. J., Whalley, L. K., Brooks, B., Goddard, A., Baeza-Romero, M. T., and Heard, D. E.: Measurements of uptake coefficients for heterogeneous loss of HO_2 onto submicron inorganic salt aerosols, *Phys. Chem. Chem. Phys.*, 15, 12829-12845, 10.1039/C3CP51831K, 2013.

Gershenzon, Y. M., Grigorieva, V. M., Ivanov, A. V., and Remorov, R. G.: O_3 and OH Sensitivity to heterogeneous sinks of HO and CH_3O_2 on aerosol particles, *Faraday Discuss.*, 100, 83-100, 10.1039/FD9950000083, 1995.

George, C., Ammann, M., and Volkamer, R.: Heterogeneous photochemistry of imidazole-2-carboxaldehyde: HO_2 radical formation and aerosol growth, *Atmos. Chem. Phys.*, 16, 11823-11836, 10.5194/acp-16-11823-2016, 2016.

Gonzalez, J., Torrent-Sucarrat, M., and Anglada, J. M.: The reactions of SO_3 with HO_2 radical and H_2O ... HO_2 radical complex. Theoretical study on the atmospheric formation of HSO_5 and H_2SO_4 , *Phys. Chem. Chem. Phys.*, 12, 2116-2125, 10.1039/B916659A, 2010.

González Palacios, L., Corral Arroyo, P., Aregahegn, K. Z., Steimer, S. S., Bartels-Rausch, T., Nozière, B., Guieu, C., Chester, R., Nimmo, M., Martin, J. M., Guerzoni, S., Nicolas, E., Mateu, J., and Keyse, S.: Atmospheric input of dissolved and particulate metals to the northwestern Mediterranean, *Deep Sea Res. (2 Top. Stud. Oceanogr.)*, 44, 655-674, 10.1016/S0967-0645(97)88508-6, 1997.

Guo, J., Tilgner, A., Yeung, C., Wang, Z., Louie, P. K. K., Luk, C. W. Y., Xu, Z., Yuan, C., Gao, Y., Poon, S., Herrmann, H., Lee, S., Lam, K. S., and Wang, T.: Atmospheric peroxides in a polluted subtropical environment: seasonal variation, sources and sinks, and importance of heterogeneous processes, *Environ. Sci. Technol.*, 48, 1443-1450, 10.1021/es403229x, 2014.

Guo, J., Wang, Z., Tao, W., and Zhang, X.: Theoretical evaluation of different factors affecting the HO_2 uptake coefficient driven by aqueous-phase first-order loss reaction, *Sci. Total Environ.*, 683, 146-153, 10.1016/j.scitotenv.2019.05.237, 2019.

Halstead, M. J. R., Cunnigham, R. G., and Hunter, K. A.: Wet deposition of trace metals to a remote site in Fiordland, New Zealand, *Atmos. Environ.*, 34, 665-676, 10.1016/S1352-2310(99)00185-5, 2000.

Hanson, D. R., Burkholder, J. B., Howard, C. J., and Ravishankara, A. R.: Measurement of hydroxyl and hydroperoxy radical uptake coefficients on water and sulfuric acid surfaces, *J. Phys. Chem.*, 96, 4979-4985, 10.1021/j100191a046, 1992.

Hanson, D. R., Ravishankara, A. R., and Solomon, S.: Heterogeneous reactions in sulfuric acid aerosols: A framework for model calculations, *J. Geophys. Res. Atmos.*, 99, 3615-3629, 10.1029/93jd02932, 1994.

Heard, D. E., and Pilling, M. J.: Measurement of OH and HO₂ in the Troposphere, *Chem. Rev.*, 103, 5163-5198, 10.1021/cr020522s, 2003.

Hennigan, C. J., Izumi, J., Sullivan, A. P., Weber, R. J., and Nenes, A.: A critical evaluation of proxy methods used to estimate the acidity of atmospheric particles, *Atmos. Chem. Phys.*, 15, 2775-2790, 10.5194/acp-15-2775-2015, 2015.

Hofmann, H., Hoffmann, P., and Lieser, K. H.: Transition metals in atmospheric aqueous samples, analytical determination and speciation, *Fresen. J. Anal. Chem.*, 340, 591-597, 10.1007/BF00322435, 1991.

Hsu, S.-C., Wong, G. T. F., Gong, G.-C., Shiah, F.-K., Huang, Y.-T., Kao, S.-J., Tsai, F., Candice Lung, S.-C., Lin, F.-J., Lin, I. I., Hung, C.-C., and Tseng, C.-M.: Sources, solubility, and dry deposition of aerosol trace elements over the East China Sea, *Mar. Chem.* 120, 116-127, 10.1016/j.marchem.2008.10.003, 2010.

J. Creasey, D., A. Halford-Maw, P., E. Heard, D., J. Pilling, M., and J. Whitaker, B.: Implementation and initial deployment of a field instrument for measurement of OH and HO₂ in the troposphere by laser-induced fluorescence, *J. Chem. Soc., Faraday Trans. 93*, 2907-2913, 10.1039/A701469D, 1997.

George, I. J., Slowik, J., and Abbatt, J.: Chemical aging of ambient organic aerosol from heterogeneous reaction with hydroxyl radicals, *Geophys. Res. Lett.*, 35, L13811, 10.1029/2008GL033884, 2008.

Jacob, D. J.: Heterogeneous chemistry and tropospheric ozone, *Atmos. Environ.*, 34, 2131-2159, 10.1016/S1352-2310(99)00462-8, 2000.

Jaeglé, L., Jacob, D. J., Brune, W. H., Faloon, I., Tan, D., Heikes, B. G., Kondo, Y., Sachse, G. W., Anderson, B., Gregory, G. L., Singh, H. B., Poeschel, R., Ferry, G., Blake, D. R., and Shetter, R. E.: Photochemistry of HO_x in the upper troposphere at northern midlatitudes, *J. Geophys. Res. Atmos.*, 105, 3877-3892, doi:10.1029/1999JD901016, 2000.

Kanaya, Y., Cao, R., Akimoto, H., Fukuda, M., Komazaki, Y., Yokouchi, Y., Koike, M., Tanimoto, H., Takegawa, N., and Kondo, Y.: Urban photochemistry in central Tokyo: 1. Observed and modeled OH and HO₂ radical concentrations during the winter and summer of 2004, *J. Geophys. Res. Atmos.*, 112, 10.1029/2007jd008670, 2007a.

Kanaya, Y., Cao, R., Kato, S., Miyakawa, Y., Kajii, Y., Tanimoto, H., Yokouchi, Y., Mochida, M., Kawamura, K., and Akimoto, H.: Chemistry of OH and HO₂ radicals observed at Rishiri Island, Japan, in September 2003: Missing daytime sink of HO₂ and positive nighttime correlations with monoterpenes, 112, 10.1029/2006jd007987, 2007b.

Lakey, P. S. J., George, I. J., Whalley, L. K., Baeza-Romero, M. T., and Heard, D. E.: Measurements of the HO₂ uptake coefficients onto single component organic aerosols, *Environ. Sci. Technol.*, 49, 4878-4885, 10.1021/acs.est.5b00948, 2015.

Lakey, P. S. J., Berkemeier, T., Krapf, M., Dommen, J., Steimer, S. S., Whalley, L. K., Ingham, T., Baeza-Romero, M. T., Pöschl, U., Shiraiwa, M., Ammann, M., and Heard, D. E.: The effect of viscosity and diffusion on the HO₂ uptake by sucrose and secondary organic aerosol particles, *Atmos. Chem. Phys.*, 16, 13035-13047, 10.5194/acp-16-13035-2016, 2016a.

Lakey, P. S. J., George, I. J., Baeza-Romero, M. T., Whalley, L. K., and Heard, D. E.: Organics substantially reduce HO₂ uptake onto aerosols containing transition metal ions, *J. Phys. Chem. A*, 120, 1421-1430, 10.1021/acs.jpca.5b06316, 2016b.

Logan, J. A., Prather, M. J., Wofsy, S. C., and McElroy, M. B.: Tropospheric chemistry: A global perspective, 86, 7210-7254, 10.1029/JC086iC08p07210, 1981.

Loukhovitskaya, E., Bedjanian, Y., Morozov, I., and Le Bras, G.: Laboratory study of the interaction of HO₂ radicals with the NaCl, NaBr, MgCl₂·6H₂O and sea salt surfaces, *Phys. Chem. Chem. Phys.*, 11, 7896-7905, 10.1039/B906300E, 2009.

Macintyre, H. L., and Evans, M. J.: Parameterisation and impact of aerosol uptake of HO₂ on a global tropospheric model, *Atmos. Chem. Phys.*, 11, 10965-10974, 10.5194/acp-11-10965-2011, 2011.

Manoj, S. V., Mishra, C. D., Sharma, M., Rani, A., Jain, R., Bansal, S. P., and Gupta, K. S.: Iron, manganese and copper concentrations in wet precipitations and kinetics of the oxidation of SO₂ in rain water at two urban sites, Jaipur and Kota, in Western India, *Atmos. Environ.*, 34, 4479-4486, 10.1016/S1352-2310(00)00117-5, 2000.

Mao, J., Jacob, D. J., Evans, M. J., Olson, J. R., Ren, X., Brune, W. H., Clair, J. M. S., Crounse, J. D., Spencer, K. M., Beaver, M. R., Wennberg, P. O., Cubison, M. J., Jimenez, J. L., Fried, A., Weibring, P., Walega, J. G., Hall, S. R., Weinheimer, A. J., Cohen, R. C., Chen, G., Crawford, J. H., McNaughton, C., Clarke, A. D., Jaeglé, L., Fisher, J. A., Yantosca, R. M., Le Sager, P., and Carouge, C.: Chemistry of hydrogen oxide radicals (HO_x) in the Arctic troposphere in spring, *Atmos. Chem. Phys.*, 10, 5823-5838, 10.5194/acp-10-5823-2010, 2010.

Mao, J., Fan, S., Jacob, D. J., and Travis, K. R.: Radical loss in the atmosphere from Cu-Fe redox coupling in aerosols, *Atmos. Chem. Phys.*, 13, 509-519, 10.5194/acp-13-509-2013, 2013a.

Mao, J., Paulot, F., Jacob, D. J., Cohen, R. C., Crounse, J. D., Wennberg, P. O., Keller, C. A., Hudman, R. C., Barkley, M. P., and Horowitz, L. W.: Ozone and organic nitrates over the eastern United States: Sensitivity to isoprene chemistry, *J. Geophys. Res. Atmos.*, 118, 211,256-211,268, 10.1002/jgrd.50817, 2013b.

Martínez, M., Harder, H., Kovacs, T. A., Simpas, J. B., Bassis, J., Leshner, R. L., Brune, W., Frost, G., Williams, E., Stroud, C., Jobson, B., Roberts, J. M., Hall, S., Shetter, R., Wert, B. P., Fried, A., Alicke, B., Stutz, J., Young, V., White, A., and Zamora, R. J.: OH and HO₂ concentrations, sources, and loss rates during the Southern Oxidants Study in Nashville, Tennessee, summer 1999, *J. Geophys. Res.*, 108, 2003.

Matthews, P. S. J., Baeza-Romero, M. T., Whalley, L. K., and Heard, D. E.: Uptake of HO₂ radicals onto Arizona test dust particles using an aerosol flow tube, *Atmos. Chem. Phys.*, 14, 7397-7408, 10.5194/acp-14-7397-2014, 2014.

Millán, L., Wang, S., Livesey, N., Kinnison, D., Sagawa, H., and Kasai, Y.: Stratospheric and mesospheric HO₂ observations from the Aura Microwave Limb Sounder, *Atmos. Chem. Phys.*, 15, 2889-2902, 10.5194/acp-15-2889-2015, 2015.

Miyazaki, K., Nakashima, Y., Schoemaeker, C., Fittschen, C., and Kajii, Y.: Note: A laser-flash photolysis and laser-induced fluorescence detection technique for measuring total HO₂ reactivity in ambient air, *Rev. Sci. Instrum.*, 84, 076106, 10.1063/1.4812634, 2013.

Morita, A., Kanaya, Y., and Francisco, J. S.: Uptake of the HO₂ radical by water: Molecular dynamics calculations and their implications for atmospheric modeling, *J. Geophys. Res. Atmos.*, 109, 10.1029/2003jd004240, 2004.

Mozurkewich, M., McMurry, P. H., Gupta, A., and Calvert, J. G.: Mass accommodation coefficient for HO₂ radicals on aqueous particles, *J. Geophys. Res. Atmos.*, 92, 4163-4170, 10.1029/JD092iD04p04163, 1987.

Nakayama, T., Matsumi, Y., Kawahito, K., Watabe, Y.: Development and evaluation of a palm-sized optical PM_{2.5} sensor. *Aerosol Sci. Technol.*, 52, 2–12, 10.1080/02786826.2017.1375078, 2018.

Ng, N. L., Canagaratna, M. R., Jimenez, J. L., Chhabra, P. S., Seinfeld, J. H., and Worsnop, D. R.: Changes in organic aerosol composition with aging inferred from aerosol mass spectra, *Atmos. Chem. Phys.*, 11, 6465-6474, 10.5194/acp-11-6465-2011, 2011.

Oakes, M., Weber, R. J., Lai, B., Russell, A., and Ingall, E. D.: Characterization of iron speciation in urban and rural single particles using XANES spectroscopy and micro X-ray fluorescence measurements: investigating the relationship between speciation and fractional iron solubility, *Atmos. Chem. Phys.*, 12, 745-756, 10.5194/acp-12-745-2012, 2012.

Remorov, R. G., Gershenzon, Y. M., Molina, L. T., and Molina, M. J.: Kinetics and mechanism of HO₂ uptake on solid NaCl, *J. Phys. Chem. A*, 106, 4558-4565, 10.1021/jp013179o, 2002.

Robinson, R. A., Stokes, R. H., and Marsh, K. N.: Activity coefficients in the ternary system: water + sucrose + sodium chloride, *J. Chem. Thermodyn.*, 2, 745-750, 10.1016/0021-9614(70)90050-9, 1970.

Ross, H. B., and Noone, K. J.: A numerical investigation of the destruction of peroxy radical by Cu ion catalysed reactions on atmospheric particles, *J. Atmos. Chem.*, 12, 121-136, 10.1007/BF00115775, 1991.

Saathoff, H., Naumann, K.-H., Riemer, N., Kamm, S., Möhler, O., Schurath, U., Vogel, H., and Vogel, B.: The loss of NO₂, HNO₃, NO₃/N₂O₅, and HO₂/HOONO₂ on soot aerosol: A chamber and modeling study, *Geophys. Res. Lett.*, 28, 1957-1960, 10.1029/2000gl012619, 2001.

Sadanaga, Y., Yoshino, A., Watanabe, K., Yoshioka, A., Wakazono, Y., Kanaya, Y., and Kajii, Y.: Development of a measurement system of OH reactivity in the atmosphere by using a laser-induced pump and probe technique, *Rev. Sci. Instrum.*, 75, 2648-2655, 10.1063/1.1775311, 2004.

Sakamoto, Y., Zhou, J., Kohno, N., Nakagawa, M., Hirokawa, J., and Kajii, Y.: Kinetics study of OH uptake onto deliquesced NaCl particles by combining Laser Photolysis and Laser-Induced Fluorescence, *J. Phys. Chem. Lett.*, 9, 4115-4119, 10.1021/acs.jpcclett.8b01725, 2018.

886 Sakamoto, Y., Sadanaga, Y., Li, J., Matsuoka, K., Takemura, M., Fujii, T., Nakagawa, M., Kohno, N.,
887 Nakashima, Y., Sato, K., Nakayama, T., Kato, S., Takami, A., Yoshino, A., Murano, K., and Kajii, Y.:
888 Relative and absolute sensitivity analysis on ozone production in Tsukuba, a city in Japan, *Environ. Sci.*
889 *Technol.*, 53, 13629-13635, 10.1021/acs.est.9b03542, 2019.

890
891 Schwarz, J. P., Spackman, J. R., Fahey, D. W., Gao, R. S., Lohmann, U., Stier, P., Watts, L. A., Thomson,
892 D. S., Lack, D. A., Pfister, L., Mahoney, M. J., Baumgardner, D., Wilson, J. C., and Reeves, J. M.:
893 Coatings and their enhancement of black carbon light absorption in the tropical atmosphere, *J.*
894 *Geophys. Res. Atmos.*, 113, 10.1029/2007JD009042, 2008.

895 Sedlak, D. L., and Hoigné, J.: The role of copper and oxalate in the redox cycling of iron in
896 atmospheric waters, *Atmos. Environ., Part A. General Topics*, 27, 2173-2185, 10.1016/0960-
897 1686(93)90047-3, 1993.

898 Siefert, R. L., Johansen, A. M., Hoffmann, M. R., and Pehkonen, S. O.: Measurements of trace metal
899 (Fe, Cu, Mn, Cr) oxidation states in fog and stratus clouds, *J. Air Waste Manage.*, 48, 128-143,
900 10.1080/10473289.1998.10463659, 1998.

901
902 Sioutas, C., Kim, S., Chang, M.: Development and evaluation of a prototype ultrafine particle
903 concentrator, *J. Aerosol Sci.* 30, 1001-1017, 10.1016/S0021-8502(98)00769-1, 1999.

904
905 Sommariva, R., Haggerstone, A. L., Carpenter, L. J., Carslaw, N., Creasey, D. J., Heard, D. E., Lee, J. D.,
906 Lewis, A. C., Pilling, M. J., and Zádor, J.: OH and HO₂ chemistry in clean marine air during SOAPEX-2,
907 *Atmos. Chem. Phys.*, 4, 839-856, 10.5194/acp-4-839-2004, 2004.

908
909 Song, H., Chen, X., Lu, K., Zou, Q., Tan, Z., Fuchs, H., Wiedensohler, A., Zheng, M., Wahner, A., Kiendler-
910 Scharr, A., and Zhang, Y.: Influence of aerosol copper on HO₂ uptake: A novel parameterized equation,
911 *Atmos. Chem. Phys. Discuss.*, 2020, 1-23, 10.5194/acp-2020-218, 2020.

912
913 Stadtler, S., Simpson, D., Schröder, S., Taraborrelli, D., Bott, A., and Schultz, M.: Ozone impacts of gas-
914 aerosol uptake in global chemistry transport models, *Atmos. Chem. Phys.*, 18, 3147-3171,
915 10.5194/acp-18-3147-2018, 2018.

916
917 Stone, D., Whalley, L. K., and Heard, D. E.: Tropospheric OH and HO₂ radicals: field measurements and
918 model comparisons, *Chem. Soc. Rev.*, 41, 6348-6404, 10.1039/C2CS35140D, 2012.

919
920 Takami, A., Mayama, N., Sakamoto, T., Ohishi, K., Irei, S., Yoshino, A., Hatakeyama, S., Murano, K.,
921 Sadanaga, Y., Bandow, H., Misawa, K., and Fujii, M.: Structural analysis of aerosol particles by
922 microscopic observation using a time-of-flight secondary ion mass spectrometer, *J. Geophys. Res.*
923 *Atmos.*, 118, 6726-6737, 10.1002/jgrd.50477, 2013.

924
925 Taketani, F., Kanaya, Y., and Akimoto, H.: Kinetics of heterogeneous reactions of HO₂ radical at
926 ambient concentration levels with (NH₄)₂SO₄ and NaCl aerosol particles, *J. Phys. Chem. A*, 112, 2370-
927 2377, 10.1021/jp0769936, 2008.

928
929 Taketani, F.; Kanaya, Y.; Akimoto, H., Heterogeneous loss of HO₂ by KCl, synthetic sea salt, and natural
930 seawater aerosol particles. *Atmos. Environ.*, **2009**, 43, (9), 1660-1665.

931
932 Taketani, F., Kanaya, Y., Pochanart, P., Liu, Y., Li, J., Okuzawa, K., Kawamura, K., Wang, Z., and Akimoto,
933 H.: Measurement of overall uptake coefficients for HO₂ radicals by aerosol particles sampled from
934 ambient air at Mts. Tai and Mang (China), *Atmos. Chem. Phys.*, 12, 11907-11916, 10.5194/acp-12-
935 11907-2012, 2012.

- Thornton, J., and Abbatt, J. P. D.: Measurements of HO₂ uptake to aqueous aerosol: Mass accommodation coefficients and net reactive loss, *J. Geophys. Res. Atmos.*, 110, 10.1029/2004jd005402, 2005.
- Thornton, J. A., Jaeglé, L., and McNeill, V. F.: Assessing known pathways for HO₂ loss in aqueous atmospheric aerosols: Regional and global impacts on tropospheric oxidants, *J. Geophys. Res. Atmos.*, 113, 10.1029/2007jd009236, 2008.
- Tie, X., Brasseur, G., Emmons, L., Horowitz, L., and Kinnison, D.: Effects of aerosols on tropospheric oxidants: A global model study, *J. Geophys. Res. Atmos.*, 106, 22931-22964, 10.1029/2001JD900206, 2001.
- Wang, Y., Arellanes, C., Curtis, D. B., and Paulson, S. E.: Probing the source of hydrogen peroxide associated with coarse mode aerosol particles in southern california, *Environ. Sci. Technol.*, 44, 4070-4075, 10.1021/es100593k, 2010.
- Wang, D., Pakbin, P., Saffari, A., Shafer, M. M., Schauer, J. J., and Sioutas, C.: Development and evaluation of a high-volume aerosol-into-liquid collector for fine and ultrafine particulate matter, *Aerosol Sci. Technol.*, 47, 1226-1238, 10.1080/02786826.2013.830693, 2013.
- Wang, D., Shafer, M. M., Schauer, J. J., and Sioutas, C.: Development of a technology for online measurement of total and water-soluble copper (Cu) in PM_{2.5}, *Aerosol Sci. Technol.*, 48, 864-874, 10.1080/02786826.2014.937478, 2014.
- Whalley, L. K., Furneaux, K. L., Goddard, A., Lee, J. D., Mahajan, A., Oetjen, H., Read, K. A., Kaaden, N., Carpenter, L. J., Lewis, A. C., Plane, J. M. C., Saltzman, E. S., Wiedensohler, A., and Heard, D. E.: The chemistry of OH and HO₂ radicals in the boundary layer over the tropical Atlantic Ocean, *Atmos. Chem. Phys.*, 10, 1555-1576, 10.5194/acp-10-1555-2010, 2010.
- Wilkinson, J., Reynolds, B., Neal, C., Hill, S., Neal, M., and Harrow, M.: Major, minor and trace element composition of cloudwater and rainwater at Plynlimon, *Hydrol. Earth Syst. Sci.*, 1, 557-569, 10.5194/hess-1-557-1997, 1997.
- You, Y., Smith, M. L., Song, M., Martin, S. T., and Bertram, A. K.: Liquid-liquid phase separation in atmospherically relevant particles consisting of organic species and inorganic salts, *Int. Rev. Phys. Chem.*, 33, 43-77, 10.1080/0144235X.2014.890786, 2014.
- Zhou, J., Elser, M., Huang, R. J., Krapf, M., Fröhlich, R., Bhattu, D., Stefenelli, G., Zotter, P., Bruns, E. A., Pieber, S. M., Ni, H., Wang, Q., Wang, Y., Zhou, Y., Chen, C., Xiao, M., Slowik, J. G., Brown, S., Cassagnes, L. E., Daellenbach, K. R., Nussbaumer, T., Geiser, M., Prévôt, A. S. H., El-Haddad, I., Cao, J., Baltensperger, U., and Dommen, J.: Predominance of secondary organic aerosol to particle-bound reactive oxygen species activity in fine ambient aerosol, *Atmos. Chem. Phys.*, 19, 14703-14720, 10.5194/acp-19-14703-2019, 2019a.
- Zhou, J., Murano, K., Kohno, N., Sakamoto, Y., and Kajii, Y.: Real-time quantification of the total HO₂ reactivity of ambient air and HO₂ uptake kinetics onto ambient aerosols in Kyoto (Japan), *Atmos. Environ.*, 117189, 10.1016/j.atmosenv.2019.117189, 2019b.